Sensors and Materials, Vol. 17, No. 1 (2005) 007–020
MYU Tokyo

S & M 0581

Measurements and Modeling of Compliance Using Novel Multi-Sensor Endoscopic Grasper

Javad Dargahi*, Siamak Najarian[1] and Xiang Zhi Zheng[2]

Mechanical and Industrial Eng., CONCAVE Research Centre, CR-200, Concordia University, Dept. of Mechanical and Industrial Eng., 1455 de Maisonneuve Blvd. West, Montreal, Quebec, Canada H3G 1M8.
[1]Mechanical and Industrial Eng., H-547-1, Dept. of Mechanical and Industrial Eng., Concordia University, 1455 de Maisonneuve Blvd. West, Montreal, Quebec, Canada H3G 1M8.
[2]Research Assistant, CONCAVE Research Centre, CR-200, Dept. of Mechanical and Industrial Eng., Concordia University, 1455 de Maisonneuve Blvd. West, Montreal, Quebec, Canada H3G 1M8.

(Received April 14, 2004; accepted October 7, 2004)

Key words: tactile sensor, compliance, endoscopic surgery, polyvinylidene fluoride

In this study, we report on the development of a new multi-sensor endoscopic grasper which is capable of measuring the sensed object's compliance and has potential applications in minimally invasive surgeries. The designed prototype has 8 cylindrical friction-enhancing projections which are supported by Plexiglas bases. The tactile sensor consists of two elements, a rigid central part and a peripheral annular-shaped compliant cylinder. Two separately located polyvinylidene fluoride (PVDF) films in the form of a circle and a ring constitute the part of the sensor that measures the applied forces. Upon contact with an object, the rigid cylinder and the compliant cylinder convey different forces to the underlying PVDF films. The relative contributions of these forces lead to the measurement of the sensed object's compliance. On the basis of the experimental data, we clarified that as the compliance of the sensed object increases, the value of the force contribution for the rigid part of the sensor decreases accordingly. Both experimental work and theoretical analysis have been carried out. The results of three-dimensional finite element modeling correspond well with experimental findings.

1. Introduction

Modern surgical procedures, such as minimally invasive surgeries (MIS), separate the surgeon's hands from the site of operation. As a result, the surgeon's perception of touch

*Corresponding author, e-mail address: jdargahi@alcor.concordia.ca

is limited to his/her visual abilities fed back from a video camera located at the end of the endoscope. The reduction of tactile sensory perception in MIS can counteract the many advantages introduced by this type of surgery, such as smaller incisions, faster recovery time, reduction of post-operation complications, and less pain.[1] The success of a minimally invasive surgery procedure depends highly upon the surgeon's ability to feel the tissues and detect the presence of blood vessels and ducts while performing the surgery.[2–6] Some special MIS techniques involve controlled manipulation tasks.[7–9] Among these techniques are: gentle load transferring during lifting, suturing tissues, grasping internal organs, and removing tissues (*e.g.*, loose bodies in knee arthroscopy and gall bladder in laparoscopic surgery).[10]

Defining the state of manipulating or gripping a biological tissue or an object requires the determination of two important physical parameters, i.e., force and position signatures.[11–13] To achieve this, different types of tactile sensors can be used to detect the presence or absence of a grasped object/tissue.[14–16] A force sensitivity extending from 0.1 N to about 10 N is normally desired in biomedical and medical robotic applications.[17]

Tissue compliance is among the vital characteristics that can be extracted from the measurements of force applied by endoscopic tools on the tissue surface. This information is extremely important to a surgeon who uses palpation to evaluate internal organs.[18] In fact, to appropriately mimic the capabilities of the human hand, any surgical tools equipped with tactile sensors should be able to measure compliance. Current endoscopic tools have different kinds of graspers for easy grasping of various slippery tissues. The jaws of these graspers normally have friction-enhancing projections, which can be modified to assist in determining the tissue compliance.

In the current work, we report on the design, fabrication, testing and modeling of a novel device by means of which the compliance of a sensed object can be determined. This modified endoscopic grasper can be potentially employed in MIS, especially in procedures where surgeons are required to manipulate the organs with extra care.

2. Previous Work

A report has been published on a modified commercial endoscopic tool in which the magnitude of the applied force was measured using strain gauges.[19] In that study, the position of the grasper was determined with the help of an optical detector. The design, fabrication and theoretical analysis of a micromachined piezoelectric tactile sensor for an endoscopic grasper have been discussed.[20] The designed sensor exhibited high force sensitivity, wide dynamic range, good linearity and high signal-to-noise ratio. The detailed finite element analysis of this sensor has also been reported.[21] An investigation on the compliance of hard rubber embedded in a block of foam using remote palpation has also been reported.[22] An endoscopic and robotic micromachined sensor has been designed and fabricated using PVDF film.[23] The development of a single tactile sensor suitable for determining the compliance of deformable objects has been presented.[24] The finite element analysis and experimental studies of this proposed sensor have also been investigated.[25] An attempt has been made to design a system in which a force-moment sensor is placed into the distal shaft of laparoscopic forceps.[26] The piezoresistive sensor array used

was a foil sensor with 64 measuring points. The pyroelectric effects associated with the PVDF-based tactile sensors were separated from the piezoelectric effect using various methods.[27] The designed device showed an alternative transient approach for distinguishing between piezoelectric and pyroelectric signals using only a single PVDF layer of film, and thereby reducing the complexity of the sensor. A report has been published on a tactile sensor assembly consisting of two semiconductor microstrain gauge sensors, which are positioned on the back face of a prototype endsocopic grasper.[28] Analysis of a membrane-type, polymeric-based tactile sensor for mapping applications in the biomedical and robotic industries has been reported.[29] Experimental and theoretical analyses of a new type of tactile sensor that can detect both the contact force and hardness of an object has been discussed.[30] In other work, modeling and measurements of the compliance of human and porcine organs have been investigated.[31]

The shortcomings of most of the current designs are mainly related to the complexity of the systems used. The major advantage of the system proposed in this paper is the simplicity and robustness of the design. Additionally, for the first time, this novel compliance sensor has been successfully incorporated into an endoscopic grasper.

3. Materials and Methods

3.1 *Design of tactile sensor*

To measure the compliance of an object placed between the jaws of an endoscopic grasper, 8 identical sensors were constructed. Each individual sensor consisted of two separate cylinders, i.e., rigid and compliant parts. Two rectangular Plexiglas supports were used as the bases for the tactile sensors. The dimensions of these supports were 24 mm × 5 mm × 2.5 mm, and the relevant mechanical properties of Plexiglas were E = 70 MPa and ν = 0.3. Figure 1 illustrates an exploded representation of the lower half of the jaw of the grasper which was equipped with 4 similar tactile sensors. For simplicity, the upper

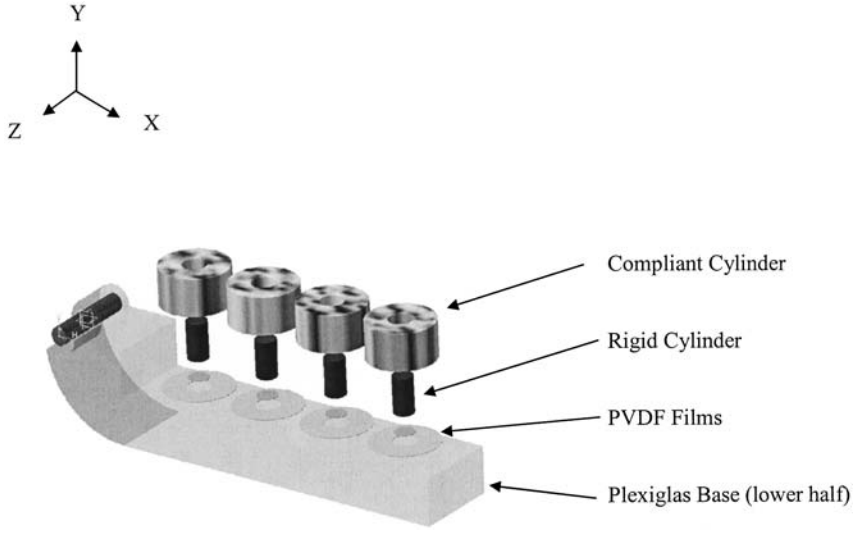

Fig. 1. Exploded illustration of the two-concentric-cylinder tactile sensors.

Plexiglas base is not shown in this figure. An important part of the designed sensor was the rigid cylinder. The purpose of this cylinder was twofold. It not only acted as a major structure in sensing the force magnitude, but also played an important role in increasing the friction between the sensed object and the grasper. High-pressure-laminated phenolic polymer was employed as the material of choice for the rigid cylinder. The phenolic polymer has excellent mechanical properties, $E = 4$ GPa and $\nu = 0.3$. The diameter of the rigid cylinder was 1.6 mm and its height was 2.025 mm. A 0.5-mm-thick metalized and poled PVDF film (Good Fellow Company, USA) in the shape of a circle was utilized as the sensing element beneath the rigid cylinder.

The second part of the sensor was a compliant cylinder which surrounded the central rigid cylinder. The outer diameter of the compliant cylinder was 4 mm, and it was the same height as the inner cylinder. There was a gap of 0.2 mm between the two concentric cylinders. Different rubber-like materials were used for the compliant cylinders with Young's moduli in the range of 2×10^4 Pa to 4×10^4 Pa. To complete the sensor, another metalized and poled PVDF film in the shape of a ring was sandwiched between the two Plexiglas bases and placed underneath the compliant cylinder. Both cylinders were glued to the Plexiglas supports. For experimental purposes and to check the total magnitude of the exerted forces, another circular PVDF film was installed in the sensor assembly.

A nonconductive glue was used to attach both the circular and annular PVDF films to the upper and lower Plexiglas supports. Two coaxial cables, each connected to one of the PVDF films, fed the output charge from the films to a charge amplifier. The system was designed so that the compliant cylinder could be readily changed. This allowed us to perform various experiments with different materials for the compliant part. One important advantage of the designed system was its thermal insulation. Due to the technique used, the system was thermally insulated from the environment. As a result of this, when the grasper was in contact with an object at a different temperature, the generated heat gradient did not lead to spurious outputs. This means that the pyroelectric effect is not a problem in the proposed design.

3.2 *Design of grasper tool*

Figure 2 illustrates a computer-generated model of the grasper. In this figure, 8 tactile sensors are located in the upper and lower grasper jaws. Each sensor was independently capable of measuring the compliance of the object placed between the jaws.

Detailed dimensions of the grasper are shown in Fig. 3. The distance between the central parts of two consecutive cylinders was chosen to be 4.5 mm (i.e., the pitch). To allow proper adjustments for the height of the two concentric cylinders a gap of 0.95 mm was provided between the jaws. In this way, cylindrical sensors of different sizes can be tested.

3.3 *Sensed objects*

A review of related literature shows that the variations of compliance and stiffness are quite large in different biological tissues. For instance, the Young's modulus of elasticity is about 0.11 MPa for the pig spleen, while it is about 4.0 MPa for the pig liver.[31–33] The same conclusion describes the case for human tissues. To cover this wide range of values,

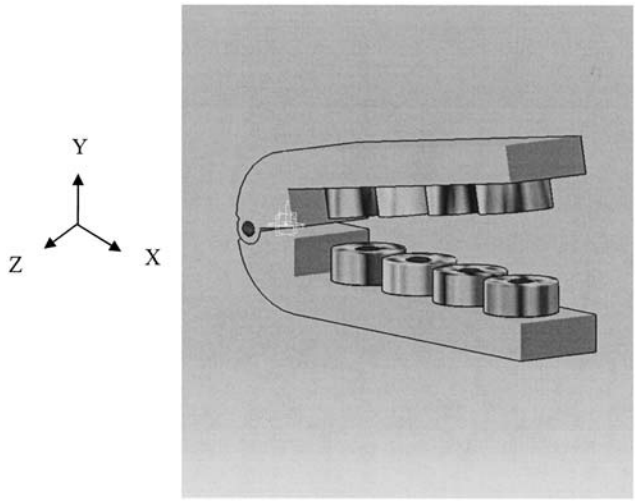

Fig. 2. Computer-generated model of the prototype grasper.

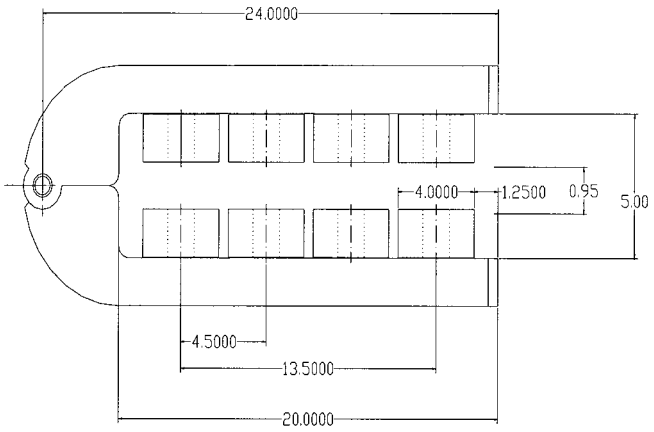

Fig. 3. Schematic drawing showing the dimensions of the grasper with cylindrical projections. All dimensions are in millimeters.

various foamed plastic and foamed rubber cylinders with a radius of 2 mm and different heights (in the range of 2–3 mm) were used. The value of E for these sensed objects were in the range of 2×10^4 to 5×10^6 Pa. Similar to soft biological tissues, soft rubber-like materials behave nonlinearly. To take this into account, the Mooney-Rivlin model was employed in the mathematical modeling of the sensed objects.

3.4 *Experimental setup*

The details of the experimental setup are represented in Fig. 4. As can be seen in this photograph, a cylindrical probe driven by a vibration unit (Ling Dynamic model 201) was used to apply a sinusoidal force at 20 Hz. The vibration unit was activated using a power amplifier and a signal generator.

Using these arrangements, it was possible to press uniformly on the entire sensed object. A force transducer (Bruel and Kjaer model 820) was used to determine the magnitude of the applied force. The force transducer was inserted between the probe and the vibration unit. A charge amplifier (D. J. Birchal model 04) was employed to amplify the charge produced by the upper circular PVDF film and the lower annular film. An oscilloscope was used to measure the resulting output. Another charge amplifier of the same type was utilized to amplify the output from the force transducer. In all runs, a dynamic load was applied to the sensed objects and the output voltage/charge values from both PVDF films and the force transducer were recorded using a chart recorder. A micropositioner was used to position the sensor relative to the location of the circular probe.

Prior to performing the experiments on objects, the sensor assembly was calibrated. The resulting calibration curve is plotted in Fig. 5. As can be observed, for the range of forces considered, i.e., 0.1 to 2 N, a good linear relationship exists between the output voltage from the sensor and the applied load on the combination of the two concentric cylinders. The correlation between voltage and force can be represented by $V = 50\ F$, where F is the applied force in newtons and V is the output voltage in millivolts.

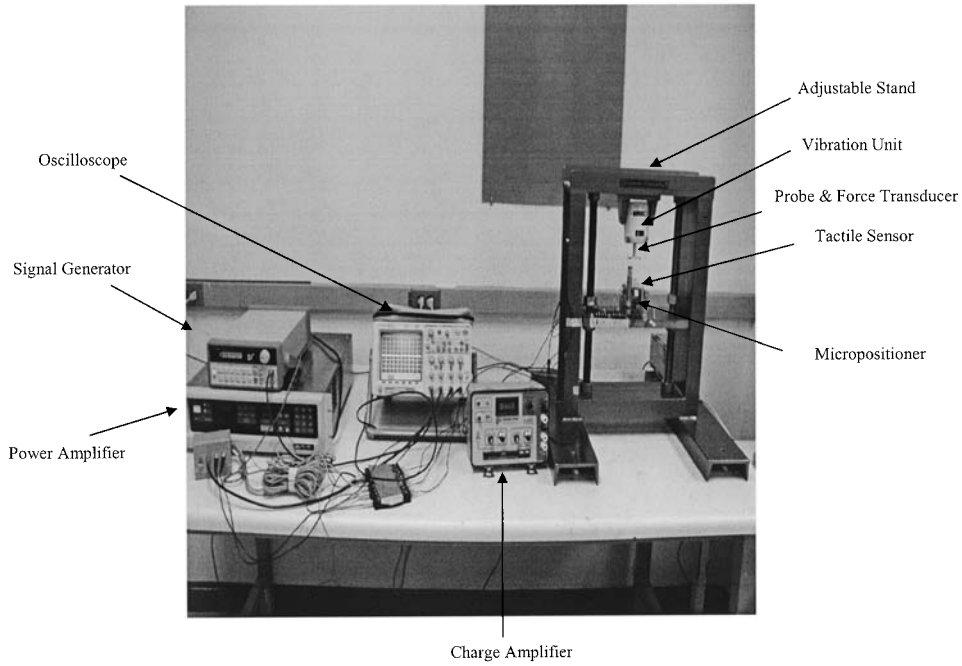

Fig. 4. Photograph of the experimental setup.

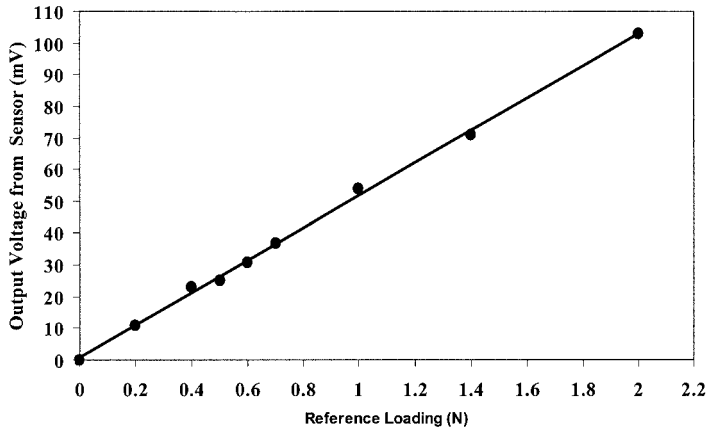

Fig. 5. Calibration curve for the tactile sensor.

After conducting preliminary runs on the grasper, a complete commercial endoscopic grasper was obtained and its jaws were replaced with the designed system. Figure 6 shows a photograph of the modified assembly which consists of four major parts: a) two grasper jaws, b) a mechanical hinge, c) a total of 8 friction-enhancing configurations, and d) a handle. Using the handle of the tool, the operator can readily actuate the rigid beam connected to the jaws via a number of solid links. By doing so, the endoscopic jaws can be closed and opened, following the forward-backward movement of the rigid beam attached to the handle. The focus of our modeling work is on the jaws of the assembly, within which the polymeric-based tactile sensors have been incorporated.

3.5 *Finite element modeling*

Three-dimensional finite element modeling was used to study the theoretical behavior of the grasper assembly. Because of the complex structure of the sensor, which consisted of various geometrical shapes with different properties, a commercial finite element analysis software package (ANSYS, version 7.1) was employed. The output of this software provided us with the magnitude of various stresses and the deformation of the tactile sensor.

Various elements were adopted for different parts of the structure. For the Plexiglas support, SOLID 45 was used, while for the PVDF films, SOLID 95 was employed. SOLID 95 was, in fact, a higher order version of the 3D 8-node solid element of SOLID 45 with the capability of tolerating irregular shapes without as great a loss of accuracy. SOLID 45 was also used for the central rigid cylinder of the sensor. For both the compliant cylinder and the sensed objects, we used HYPER 58 elements. While SOLID 45 elements are more appropriate for 3D structural solids, HYPER 58 elements are more suitable for 3D hyperelastic solids. The use of nonlinear analysis with HYPER 58 was necessary, although it increased the computing time noticeably because of the large deformations in the rubber-like materials of the sensed objects and the compliant cylinder. To simulate the behavior of these parts, the Mooney-Rivlin model was adopted in the FEM. In this model, the strain energy density function (W) is defined in terms of input parameters c_{10}, c_{01}, and d:

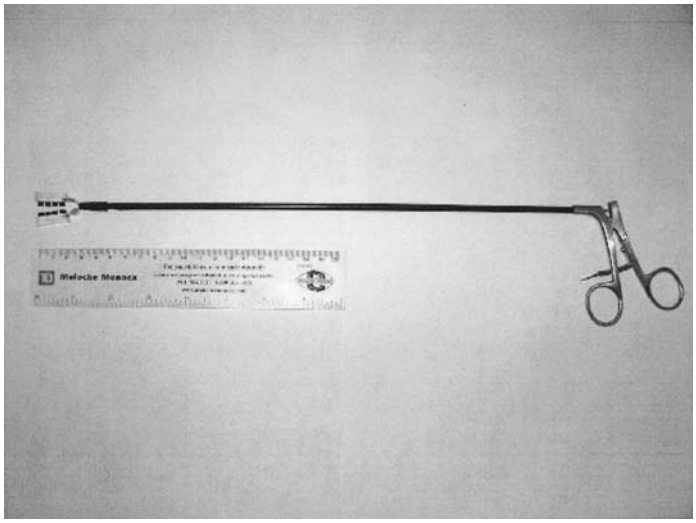

Fig. 6. Photograph of a complete endoscopic grasper equipped with modified jaws.

$$W = c_{10}\left(\bar{I}_1 - 3\right) + c_{01}\left(\bar{I}_2 - 3\right) + \frac{1}{d}\left(J_{el} - 1\right)^2, \tag{1}$$

where c_{10}, c_{01}, and d are the material constants, $\bar{I}_1$ and $\bar{I}_2$ are the invariants of the right Cauchy-Green tensor, and J_{el} is the elastic volumetric deformation. Typical values used in the modeling are $c_{10} = 0.177 \times 10^6$ Pa, $c_{01} = 0.65 \times 10^6$, and $d = 333 \times 10^6$ Pa. On the basis of the Mooney-Rivlin model, an approximate value for the Young's modulus of elasticity can be obtained using $E \approx 6(c_{10} + c_{01})$.

With regard to PVDF films, the beta phase of PVDF has a C_{2v} crystal symmetry, and its piezoelectric coefficient can be denoted by the following 3×6 matrix:[34]

$$d_{ij} = \begin{bmatrix} 0 & 0 & 0 & 0 & d_{15} & 0 \\ 0 & 0 & 0 & d_{24} & 0 & 0 \\ d_{31} & d_{32} & d_{33} & 0 & 0 & 0 \end{bmatrix}$$

When a sinusoidal force is applied to the PVDF sensor, the output charge from each PVDF sensing element is, in effect, a combination of the sum of the piezoelectric coefficients d_{31}, d_{32}, and d_{33} in the drawn, transverse, and thickness directions, respectively, multiplied by the magnitude of the applied force. In mathematical form, we have:

$$F = \frac{q}{\psi_1 d_{31} + \psi_2 d_{32} + d_{33}}, \tag{2}$$

where q is the output charge, F is the applied force on a sensing element, and ψ_1 and ψ_2 are constants proportional to the electrode area of the sensing elements. Table 1 summarizes the piezoelectric coefficients of the PVDF together with its mechanical properties, on the basis of the manufacturer's technical specifications. The piezoelectric coefficients are presented in both pC/N (d-form) and Vm/N (g-form) units.

In the FEM, the total number of elements produced, after meshing the whole structure, was 7,010. Further refinement of the number of elements did not produce any significant improvement in the modeling results. Therefore, from a modeling point of view, the generated mesh proved to be sufficiently accurate for the purpose of this study. The meshing adopted for the lower half of the system is shown in Fig. 7.

4. Results and Discussion

Different modes of loading conditions were used, such as applying different loads on the cylindrical projections. However, for the sake of brevity, only one of the cases in which a load of 1 N is applied on the first projection is presented. Keeping the magnitude of applied force at 1 N, various objects with different moduli of elasticity were placed between the jaws. Depending on the compliance of the sensed object, the ratio of force

Table 1
Material specifications of PVDF.

Piezoelectric Coefficients				Young's Modulus(GPa)	
d-from(pC/N)		g-form(Vm/N)			
d_{31}	18–20	g_{31}	0.15	E_x	2.25
d_{32}	2	g_{32}	0.015	E_y	2.20
d_{33}	–20	g_{33}	–0.15		

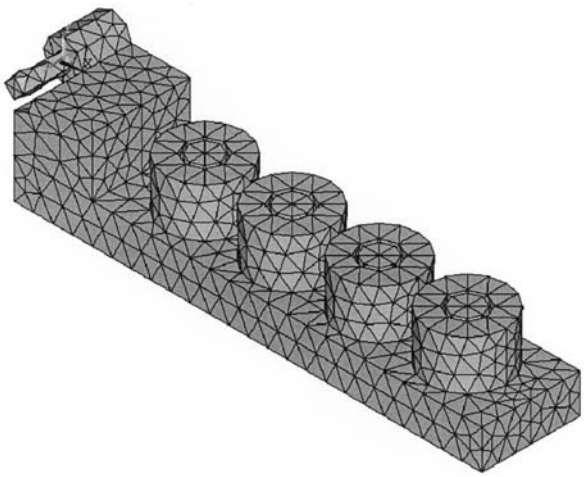

Fig. 7. Mesh produced by finite element modeling.

exerted on the rigid cylinder to the force exerted on the compliant cylinder varied considerably. To analyze the data, the following parameters were applied:

- *Force Ratio:* This is the ratio of the force applied on the rigid cylinder to the total applied force, i.e., $F_R / (F_R + F_C)$. In this dimensionless parameter, F_R is the rigid cylinder force and F_C is the compliant cylinder force.
- *Object Compliance:* This parameter is an indication of the sensed object's compliance and is denoted as δ_O / E_O. Here, E_O is the stiffness of the object and δ_O is its thickness.
- *Compliant Cylinder Compliance:* Similarly, this describes the compliance of the compliant part of the sensor and is defined as δ_C / E_C. The stiffness and thickness of the compliant cylinder are represented by E_C and δ_C, respectively.
- *Combined Compliance Ratio:* This is a dimensionless parameter which gives an indication of the relative importance of the compliance of the compliant part with respect to the compliance of the sensed object. It is denoted as $(\delta_C / E_C)/(\delta_O / E_O)$.

Figure 8 shows the experimental results obtained when the combined compliance ratio was varied from 1 to 32. On the basis of these data, we can see that as the combined compliance ratio increases, the force ratio increases as well. This means that lower compliance values for the sensed object result in the exertion of higher forces on the rigid part of the sensor. According to this figure, up to a value of about 16 for $(\delta_C / E_C)/(\delta_O / E_O)$, the force ratio increases sharply. However, beyond this threshold, the steepness of the curve decreases significantly. It can be predicted that the value of force ratio approaches unity asymptotically. This is verified by the trend in the experimental data as well.

To study the contribution of the compliant cylinder, different runs with various compliances for this cylinder were performed. The experimental results are presented in Fig. 9. For a fixed value of δ_O / E_O, an increase in the value of compliance for the compliant cylinder leads to an increase in the contribution of forces received by the rigid cylinder. The role of the compliant element of the sensor was tested for two different values of δ_C / E_C, i.e., 50 and 100 m/MPa. At an object compliance of 5 m/MPa, a 20% rise in force ratio is observed when δ_C / E_C is increased from 50 to 100 m/MPa.

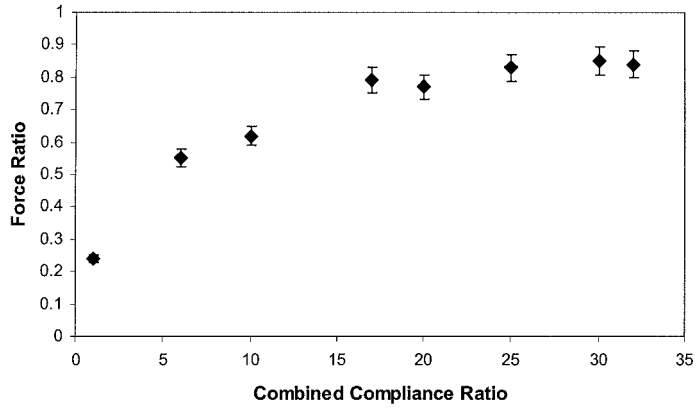

Fig. 8. Experimental data showing the variation of the force ratio with the combined compliance ratio.

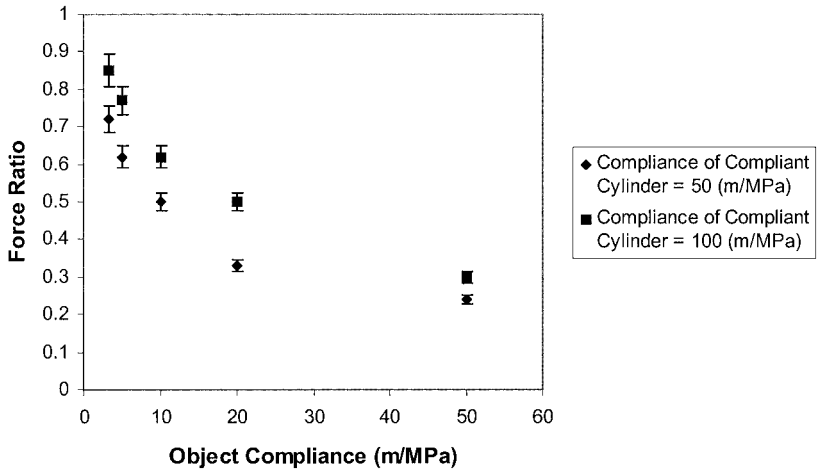

Fig. 9. Effect of compliance of compliant cylinder on the force ratio.

The major focus of this work was on the analysis used in the study of the soft tissues, and that is why a range of 3.3 to 50 m/MPa for the sensed object compliance was covered experimentally. For stiffer tissues, it is expected that at low values of δ_O / E_O the force ratio will approach unity, regardless of δ_C / E_C values. Errors involved in the experimental arrangement were difficult to quantify theoretically, but a reproducibility of about 5% was estimated for the force ratio from repeated measurements.

With regard to the mathematical modeling of the system and to predict the contribution of forces on each part of the sensor, various stresses were computed. To achieve this, the entire grasper was meshed and the output voltages from the two PVDF films were determined. The results that were used in calculating the output voltage, and hence the force ratio, were extracted from the stresses in the PVDF films. Figure 10 presents the model employed in the finite element analysis for both the circular and the annular PVDF films.

All four stresses, σ_x, σ_y, σ_z, and σ_{von} (von Mises stress), were computed and, as expected, the predominant normal stress is the component in the *y*-direction (i.e., the vertical direction). Taking into account the simulated results, the theoretical output voltage can be obtained from the following equation:

$$V_o = \sum_{i=1}^{3} g_{3i} \cdot \sigma_i \cdot t, \tag{3}$$

where V_o is the output voltage in volts, t is the PVDF thickness in meters, σ_i ($i = x, y, z$ or *1*, *2*, *3*) are the normal stresses in Pascals, and g_{3i} ($i = 1, 2, 3$) are the piezoelectric coefficients in Vm/N. Knowing the value of t (which is 25 μm) and the g_{3i} values from Table 1, the output voltage was computed, using the simulated values of σ_x, σ_y, and σ_z. Because the stress magnitudes vary in the radial direction, average values were used by integrating σ_i

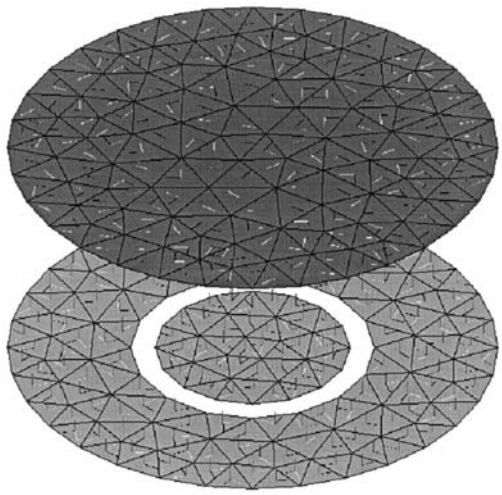

Fig. 10. Geometrical model of the PVDF films.

with respect to the surface area of the films. For instance, $\sigma_{y,\,average}$ was computed as, $\int \sigma_y . dA / \int dA$, where A denotes the surface area of the corresponding geometry, i.e., a ring-shaped or a circular film. Figure 11 presents the simulated results obtained together with the corresponding experimental data. For the range of combined compliance ratios which was tested experimentally, a good correspondence was obtained between the experimental data and the theoretical predictions. An average error of 25% was observed in the predicted force ratio using the finite element method.

5. Summary and Conclusions

Using the prototype endoscopic grasper, it is possible to readily measure the compliance of various soft objects, including biological tissues. A major advantage of the designed system is that it can be easily miniaturized and micromachined. As a result, it could be mass-produced at low cost and even be disposable.

Another feature of the designed prototype involves the polarization characteristics of the PVDF polymers. It is well known that, in PVDF polymers, polarization can be changed both by mechanical stress and by temperature variation. The former is associated with the piezoelectric property of this polymer, and the latter with the pyroelectric effect. In the design of the sensor, care has been taken to avoid the pyroelectric effect. To achieve this, the PVDF film was sandwiched between Plexiglas layers, which successfully eliminated the pyroelectric contribution of the film.

Three-dimensional finite element modeling has proven to be a powerful tool in predicting the theoretical characteristics of the endoscopic grasper. The advantage of the 3D analysis is more pronounced when an object or a biological tissue with nonuniform three dimensional geometry is grasped by the jaws. Here, the load distribution has a relatively complex form. However, even in these cases, the use of the proposed method is straightforward and the fundamental concept remains the same.

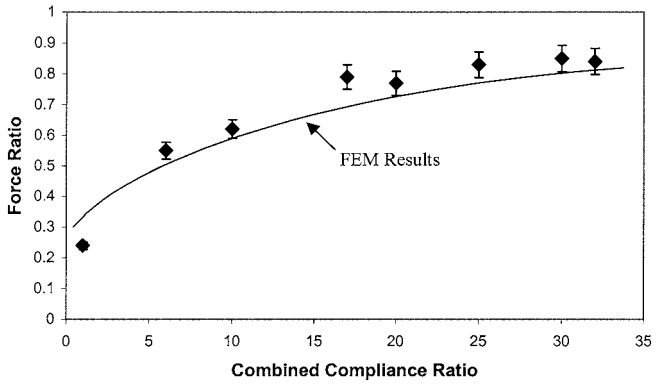

Fig. 11. Comparison of experimental data and theoretical results obtained by FEM.

In the designed system, a gap of 0.2 mm was allocated between the compliant and rigid cylinders. The reason for this gap was to eliminate friction between the two concentric cylinders and hence to make the sensor operate more smoothly. Gaps larger than the prescribed value made the device less robust. In the current work, no attempt was made to optimize the size of the cylindrical projections; however, it is predicted that by scaling down the system, the performance will not be affected.

Work is currently underway in our lab to investigate the experimental studies and theoretical modeling for cases in which soft tissues with more complex geometries are grasped by this prototype system.

Acknowledgments

Our special thanks go to Dr. H. Scarth (the Chief Surgeon at Saint John Regional Hospital, Saint John, Canada) for his valuable comments and suggestions on the clinical aspects of this research. Furthermore, the authors thank the Institute for Robotics and Intelligent Systems (IRIS) and Natural Sciences and Engineering Research Council (NSERC) of Canada for providing the financial support for this project.

References

1 I. Brouwer, J. Ustin, L. Bentley, A. Sherman, N. Dhruv and F. Tendick: Medicine Meets Virtual Reality **81 (**2001) 69.
2 J. Dargahi and S. Najarian: Bio-Medical Materials and Engineering **14** (2004) 151.
3 J. Dargahi and S. Najarian: Sensor Review **24** (2004) 284.
4 P. Dario: Sensors and Actuators A **26 (**1991) 251.
5 J. Dargahi, A. Eastwood and I. J. Kemp: International Conference on Sensor Fusion: Architectures Algorithms and Applications 1997 (SPIE, Orlando, 1997) p. 20.
6 J. Dargahi, M. Parameswaran and S. Payandeh: Journal of Microelectromechanical Systems **9** (2000) 329.
7 J. Dargahi and S. Payandeh: International Conference on Sensor Fusion: Architectures Algorithms and Applications 1998 (SPIE, Orlando, 1998) p. 122.

8 A. Fisch, C. Mavroidis, J. M. Huber and Y. B. Cohen: Haptic Devices for Virtual Reality, Telepresence, and Human-Assistive Robotics, Biologically-Inspired Intelligent Robots, ed. Y. B. Cohen and C. Breazeal (SPIE Press, Bellingham, 2003) p. 5.
9 J. Dargahi: Sensors and Actuators A **80** (2000) 23.
10 H. H. Melzer, M. O. Schurr, W. Kunert, G. Buess, U. Voges and J. U. Meyer: Endoscopic Surgery and Allied Technologies **1** (1993) 165.
11 B. Gray and R. S. Fearing: International Conference on Robotics and Automation 1996 (IEEE, Minneapolis, 1996) p. 1.
12 E. S. Kolesar, P. R. Reston, D. G. Ford and R. C. Fitch: Journal of Robotic Systems **9** (1992) 37.
13 M. H. Lee and H. R. Nicholls: Mechateronics **9** (1999) 1.
14 B. Hannaford, J. Trujillo, M. Sinanan, M. Moreyra, J. Rosen, J. Brown, R. Leuschke and M. MacFarlane: Medicine Meets Virtual Reality **50** (1998) 265.
15 N. P. Rao, J. Dargahi, M. Kahrizi and S. Prasad: Canadian Conference on Electrical and Computer Engineering 2003 (CCECE, Montreal, 2003).
16 J. Dargahi: CSME International Conference 2001 (CSME, Montreal, 2001) p. 21.
17 E. Crago, J. Nakai and H. J. Chizeck: IEEE Transactions on Biomedical Engineering **38** (1991) 17.
18 T. A. Krouskop, T.M. Wheeler, F. Kallel, B.S. Garra and T. Hall: Ultrasonic Imaging **20** (1998) 260.
19 A. Bicchi, G. Canepa, D. De Rossi, P. Iacconi and E.P. Scilingo: International Conference on Robotics and Automation 1996 (IEEE, Minneapolis, 1996) p. 884.
20 J. Dargahi, M. Normandeau, J. Milne, M. Parameswaran and S. Payandeh: International Conference on Sensor Fusion: Architecture, Algorithms, and Applications 2000 (SPIE, Orlando, 2000) p. 349.
21 J. Dargahi and S. Najarian: Sensor Review **24** (2004) 74.
22 R. D. Howe, W. J. Peine, D.A. Kontarinis and J. S. Son: IEEE Engineering in Medicine and Biology Magazine **14** (1994) 318.
23 J. Dargahi, S. Payandeh and M. Parameswaran: International Conference on Robotics and Automation 1999 (IEEE, Detroit, 1999) p. 299.
24 J. Dargahi: Journal of Mechanical Design **124** (2002) 576.
25 H. Singh, J. Dargahi and R. Sedaghati: 2nd International Conference on Sensors 2003 (IEEE, Toronto, 2003).
26 H. Fischer, B. Neisius and R. Trapp: Tactile feedback for endoscopic surgery, Interactive Technology and a New Paradigm for Health Care, ed. K. Morgan, M. Satava, B. Sieburg, R. Mattheus and J. P. Christensen (IOS Press, Amsterdam,1995) p. 114.
27 J. Dargahi: Sensor and Actuators A **71** (1998) 89.
28 J. Dargahi and S. Najarian: Canadian Journal of Electrical and Computer Engineering **28** (2003) 155.
29 J. Dargahi and S. Najarian: Sensors and Materials **16** (2004) 25.
30 M. Shikida, T. Shimizu, K. Sato and K. Itoigawa: Sensors and Actuators A **103** (2003) 213.
31 F. J. Carter, T. G. Frank, P. J. Davies, D. McLean and A. Cuschieri: Medical Image Analysis **5** (2001) 231.
32 Y. Uchio, M. Ochi, N. Adachi, K. Kawasaki and J. Iwasa: Medical Engineering & Physics **24** (2002) 431.
33 Y. B. Choy, H. Cao, S. Tungjitkusolmun, J. Z. Tsai, D. Haemmerich, V. R. Vorperian and J. G. Webster: Journal of Biomechanics **35** (2002) 1671.
34 J. Dargahi: The application of polyvinylidene fluoride as a robotic tactile sensor, Ph.D. Dissertation, Glasgow Caledonian University, Glasgow, Scotland (1993).